Sensitivity of Z+jet production data to the gluon PDF

Summer student progress report by

Aaron Gootjes-Dreesbach

TU Dortmund

supervised by Pavel Starovoitov

September 2014

Abstract

This report describes my work during the 2014 summerstudent programme at DESY Hamburg. The APPLgrid method for inclusion of PDFs in QCD calculations is presented and applied to Z+jet production at next to leading order. Using this, the sensitivity of recent ATLAS data on the rapidity distribution of Z+jet production to the gluon PDF is investigated by calculating subprocess contributions and correlations. We find a strong correlation at high and medium x for the leading jet that warrants further studies.

Contents

1 Introduction

Reducing the uncertainties in the parton distribution functions (PDFs) of the proton is essential to enable precision measurements at hadron colliders like the LHC. Especially the gluon PDF suffers from large uncertainties in some regions of the fractional momentum x.

Precision data on Drell-Yan and inclusive jet production at Tevatron and the LHC is already used for this purpose. They are used in PDF fits of a number of collaborations, such as NNPDF [1], CT10 [2] and MSTW2008 [3]. This motivates the investigation into the sensitivity of Z+jet production to the gluon PDF, which is the central issue examined in this work. For this purpose, the APPLgrid [4] software package is used with `MCFM 6.8` [5] to generate a grid for the fast evaluation of cross sections from varied input PDF sets. Experimental measurements of this process were published by the ATLAS Collaboration, using their 2011 dataset at a center-of-mass energy of 7 TeV [6].

This report describes the work I did as part of the 2014 summer student programme at DESY Hamburg under the supervision of Pavel Starovoitov at the DESY ATLAS group.

It is organized as follows: In the rest of this section, I will discuss the theoretical background of PDFs and the APPLgrid project as the central tool I used for my investigation. In sections 2 and 3, I will present the subprocess decomposition I implemented for Z+jet production at NLO and go into detail about the grid generation itself. In the last section, I will describe my results, including a comparison to ATLAS data as well as an analysis of the gluon PDF contributions and correlations.

1.1 The factorisation theorem and Parton Distribution Functions

The central theoretical concept that allows one to use perturbative QCD for the calculations of hadronic processes despite the inherently non-perturbative nature of hadronization is called the factorisation theorem. It separates a calculation into perturbatively calculable short-distance components and universal long-distance components that can be measured experimentally. One formulation of this for two interacting hadrons is given in Eq. (1):

$$\sigma = \sum_{i,j} \int \mathrm{d}x_1 \mathrm{d}x_2 \;\; f_{i/H1}(x_1, \mu_F^2)\; f_{j/H2}(x_2, \mu_F^2) \;\; \sigma_{ij}(\alpha_s(\mu_R^2), x_1 x_2 s, \mu_F^2), \qquad (1)$$

where μ_R and μ_F are the renormalization and factorisation scale, respectively, α_s is the strong coupling and σ_{ij} is the cross section for the hard process. This equation holds at sufficiently large energies and introduces the parton distribution functions

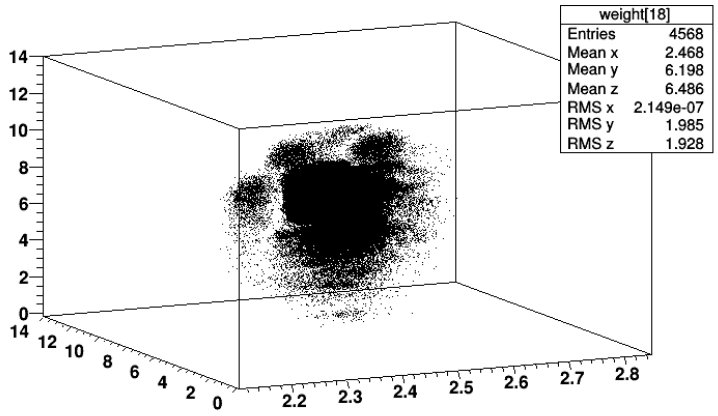

FIG. 1. Visualization of a grid, where two axes correspond to fractional parton momenta and the third to the factorisation scale.

$f_{i/HX}(x, Q^2)$, where i ist the type of parton it is related to and HX is one of the two interacting particles. These can be visualized as the number density to find a parton carrying a fraction x of the total hadron momentum at an energy scale Q^2. While at low energies, the valence quarks lead to a high probability to find these with roughly one third of the momentum, a high number of gluons and sea quarks with low x dominate at high energies.

PDFs can be extracted from structure function data. These can be measured experimentally, most importantly through deep inelastic scattering experiments and with data from the electron-proton collider HERA at DESY. The dependency of the PDFs on the energy scale Q^2 can be calculated theoretically using the DGLAP evolution equation (e.g. [7]), which makes a combination of experimental data at different energy scales possible.

Factorisation in pQCD is discussed in much more detail elsewhere, e.g. [8].

1.2 The applgrid project

The APPLgrid project, which is described in detail in [4], provides a method to generate interpolation grids with Monte Carlo event generators that can subsequently be convoluted with different PDFs and strong couplings to quickly evaluate cross sections. Additionally, it allows the variation of renormalization and factorisation scales. Currently, interfaces for grid generation exist for `MCFM` and `NLOJet++`.

The interpolation grid stores the weights for the hard, perturbative process as a function of the two interacting parton's fractional momenta x_1 and x_2 as well as the energy scale Q^2. A variable transformation is applied to these to get a uniform coverage of the full kinematic spectrum. Figure 1 shows a visualization of such a grid.

Since different combinations of interacting partons can carry different weights and we usually want to obtain the cross section in a number of bins, such a grid is created for every combinations of these. The decomposition of all parton combinations into subprocesses with common weights can be done manually or, after the grid generation, automatically and will be discussed for Z+jet production in section 2.

Finally, to be able to vary the strong coupling and renormalization scale, leading order and next to leading order contributions are stored separately as well.

APPLgrid uses a custom data structure that requires two runs of the event generator, where the first run determines the phase space to optimize boundaries of the grids. Only the second run stores the event weights in the optimized grids.

For the inclusion of current PDF sets, `LHAPDF 6.1.3` [9] was used. For arbitrary variation of the factorisation scale, APPLgrid utilises an implementation of the DGLAP evolution equation from `HOPPET 1.1.5` [10].

2 Subprocess decomposition

In order to both speed up the grid generation and reduce the required memory, it is neccessary to identify which combinations of interacting partons contribute with the same weights and thereby which subprocess grids carry redundant information. To derive such a subprocess decomposition for Z+jets at next to leading order, we first consider an existing decomposition for Z production [4], which is given in Table I.

ID		**Process**	**Category**
0	$U\bar{U}:$	$\sum_{i=2,4,6} f_{i/H1} f_{-i/H2}$	4×**quark-antiquark** processes (same flavour)
1	$D\bar{D}:$	$\sum_{i=1,3,5} f_{i/H1} f_{-i/H2}$	
2	$\bar{U}U:$	$\sum_{i=2,4,6} f_{-i/H1} f_{i/H2}$	
3	$\bar{D}D:$	$\sum_{i=1,3,5} f_{-i/H1} f_{i/H2}$	
4	$gU:$	$\sum_{i=2,4,6} f_{0/H1} f_{i/H2}$	8×**quark-gluon** processes
5	$g\bar{U}:$	$\sum_{i=2,4,6} f_{0/H1} f_{-i/H2}$	
6	$gD:$	$\sum_{i=1,3,5} f_{0/H1} f_{i/H2}$	
7	$g\bar{D}:$	$\sum_{i=1,3,5} f_{0/H1} f_{-i/H2}$	
8	$Ug:$	$\sum_{i=2,4,6} f_{i/H1} f_{0/H2}$	
9	$\bar{U}g:$	$\sum_{i=2,4,6} f_{-i/H1} f_{0/H2}$	
10	$Dg:$	$\sum_{i=1,3,5} f_{i/H1} f_{0/H2}$	
11	$\bar{D}g:$	$\sum_{i=1,3,5} f_{-i/H1} f_{0/H2}$	

TABLE I. Subprocess decomposition for Z production at NLO [4]. U, D and g denote an up-type quark, down-type quark and gluon, respectively. The third column gives an expression for a generalized PDF specific to each subprocess, where $f_{i/Hj}$ stands for the PDF of a parton with flavour i in the j-th hadron.

The criteria by which the 169 possible parton combinations are distributed into these 12 subprocesses are the following: First of all, the Z boson can be produced by either a quark-antiquark Drell-Yan process or radiated by the quark in a quark-gluon process. These categories are subdivided by the charge of the quarks to account for the

coupling of an off-shell photon. To allow for the treatment of asymmetric machines, we additionally distinguish by the order of interacting partons.

ID		Process	Category
12	$gg:$	$f_{0/H1} \cdot f_{0/H2}$	1×**gluon-gluon** process
13	$UU':$	$\sum_{i,j=2,4,6;\ i\neq j} f_{i/H1} f_{j/H2}$	16×**quark-quark** processes (different flavours)
14	$DU:$	$\sum_{i=1,3,5;\ j=2,4,6} f_{i/H1} f_{j/H2}$	
15	$\bar{U}U':$	$\sum_{i,j=2,4,6;\ i\neq j} f_{-i/H1} f_{j/H2}$	
16	$\bar{D}U:$	$\sum_{i=1,3,5;\ j=2,4,6} f_{-i/H1} f_{j/H2}$	
17	$UD:$	$\sum_{i=2,4,6;\ j=1,3,5} f_{i/H1} f_{j/H2}$	
18	$DD':$	$\sum_{i,j=1,3,5;\ i\neq j} f_{i/H1} f_{j/H2}$	
19	$\bar{U}D:$	$\sum_{i=2,4,6;\ j=1,3,5} f_{-i/H1} f_{j/H2}$	
20	$\bar{D}D':$	$\sum_{i,j=1,3,5;\ i\neq j} f_{-i/H1} f_{j/H2}$	
21	$U\bar{U}':$	$\sum_{i,j=2,4,6;\ i\neq j} f_{i/H1} f_{-j/H2}$	
22	$D\bar{U}:$	$\sum_{i=1,3,5;\ j=2,4,6} f_{i/H1} f_{-j/H2}$	
23	$\bar{U}\bar{U}':$	$\sum_{i,j=2,4,6;\ i\neq j} f_{-i/H1} f_{-j/H2}$	
24	$\bar{D}\bar{U}:$	$\sum_{i=1,3,5;\ j=2,4,6} f_{-i/H1} f_{-j/H2}$	
25	$U\bar{D}:$	$\sum_{i=2,4,6;\ j=1,3,5} f_{i/H1} f_{-j/H2}$	
26	$D\bar{D}':$	$\sum_{i,j=1,3,5;\ i\neq j} f_{i/H1} f_{-j/H2}$	
27	$\bar{U}\bar{D}:$	$\sum_{i=2,4,6;\ j=1,3,5} f_{-i/H1} f_{-j/H2}$	
28	$\bar{D}\bar{D}':$	$\sum_{i,j=1,3,5;\ i\neq j} f_{-i/H1} f_{-j/H2}$	
29	$UU:$	$\sum_{i=2,4,6} f_{i/H1} f_{i/H2}$	4×**quark-quark** processes (same flavour)
30	$DD:$	$\sum_{i=1,3,5} f_{i/H1} f_{i/H2}$	
31	$\bar{U}\bar{U}:$	$\sum_{i=2,4,6} f_{-i/H1} f_{-i/H2}$	
32	$\bar{D}\bar{D}:$	$\sum_{i=1,3,5} f_{-i/H1} f_{-i/H2}$	

TABLE II. Additional subprocesses for Z+jet production. Details are as in Table I.

All the processes listed for Z production also contribute to Z+jets, since any parton can radiate a gluon in the final state. However, a number of additional processes become possible through the added jet. These are given in Table II and consist of a gluon-gluon process, 16 quark-quark processes where the two quarks have different flavours and 4 quark-quark processes where they have the same. This additional

subdivision is neccessary to account for processes like annihilation, which are only possible for identical quark flavour.

This decomposition was implemented in two different ways: As `c++` code compiled into APPLgridand as a `.config` file.

The very small discrepancy between grid and reference calculation that will be discussed in detail in section 3.4 is a strong indication that this subprocess decomposition is correct. Moreover, by applying APPLgrid's automated method of reducing the number of processes after the grid generation, the decomposition turns out to be optimal, since it is not reduced through this step.

3 Grid generation

For the grid generation, the parton-level Monte Carlo event generator `MCFM 6.8` is used, whose implementation of Z+jet production is described in [5]. This requires `FastJet 3.0.6` [11] for the jet finding algorithm and a patch that includes the interface library `mcfm_bridge`, which is responsible for recording the weights. This section will provide details on the grid generation procedure.

3.1 Interfacing `MCFM`

To be able to use the latest version of `MCFM`, a number of minor changes had to be implemented. These included updating the value of `mxpart`, the maximal number of partons, to `14` as well as editing the `MCFM` patch to account for a number of added source files in this release.

The interface implements a binning of the cross section in 18 bins of the rapidity $|y^{jet}|$ of either the leading or subleading jet between 0 and 4.4, corresponding to the binning used in [6]. The grid parameters used for this calculation are determined by the interface as well and listed in Table III.

Minimal x	$x_{min} = 10^{-9}$
Maximal x	$x_{max} = 1$
Number of bins of x	$N_x = 40$
x interpolation order	$k_x = 6$
Minimal Q^2	$Q^2_{min} = 1$ GeV^2
Maximal Q^2	$Q^2_{max} = 16$ TeV^2
Number of bins of Q^2	$N_{Q^2} = 15$
Q^2 interpolation order	$k_{Q^2} = 3$
Transform parameter a	$a = 5$

TABLE III. Grid parameters used for these calculations. Details on their effects can be found in [4].

3.2 `MCFM` configuration

`MCFM` is configured through a steering file called `"input.DAT"`. This section gives an overview of the most important parameters but the full file used for the generation of these grids can be found in the appendix.

The choice `nproc=41` corresponds to the NLO calculation of the production of a Z boson and at least one jet, where the Z subsequently decays into electrons and effects

from γ^* production are accounted for. To be able to compare the calculated cross sections to data, many parameters are chosen to match those in the ATLAS analysis [6]. This includes the center of mass energy of 7 TeV, the applied cuts, which are listed in Table IV, and the jet definition resulting from the anti-k_T algorithm [12] with $R = 0.4$.

lepton p_T	$p_T > 20$ GeV
lepton $\|\eta\|$	$\|\eta\| < 1.37$ $v.$ $1.52 < \|\eta\| < 2.47$
lepton separation ΔR^{ll}	$\Delta R^{ll} > 0.2$
lepton invariant mass m^{ll}	66 GeV $\leq m^{ll} \leq$ 116 GeV
jet p_T^{jet}	$p_T^{jet} > 30$ GeV
jet $\|y^{jet}\|$	$\|y^{jet}\| < 4.4$
jet-lepton separation ΔR^{lj}	$\Delta R^{lj} > 0.5$

TABLE IV. Summary of cuts applied to the generated events [6], where $\Delta R = \sqrt{\Delta\phi^2 + \Delta\eta^2}$.

The factorisation and renormalization scales are set to the fixed value of the Z boson mass. While smaller samples were calculated using a dynamic scale proportional to the scalar sum of transverse momenta, these led to differences of up to 2% between standard and grid calculation. Apart from this, however, the smaller samples show a very similar behaviour in the rest of the analysis.

While this does not affect the calculated grid, the CT10 PDF was used during the calculation.

3.3 Running the generation jobs

The calculation of the grids was performed entirely on the DESY batch infrastructure BIRD using Scientific Linux 6 and a number of custom automated job submission scripts. For a fast calculation, the total sample size of approximately 200 billion events was distributed on 200 copies. The generation is divided into four steps:

1. 1st run of `MCFM` for each of the copies to determine the phase space and write optimized grids.

2. Combination of all phasespace grids using `applgrid-combine`.

3. 2nd run of `MCFM` for each copy reads in the test grids and fills them with event weights.

4. Combination of weight grids into final result.

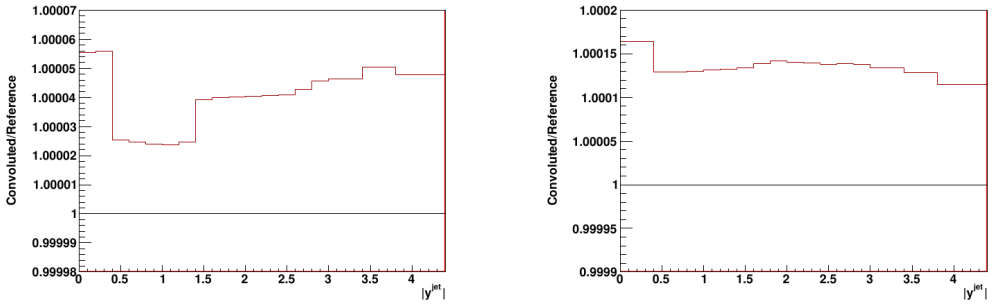

(a) Leading jet (b) Subleading jet

FIG. 2. Ratio plot between grid and standard calculation of the Z+jet cross section in bins of the rapidity of leading and subleading jet.

3.4 Checks of the grid calculation

During the grid generation, a reference histogram of the normal `MCFM` calculation is stored as well. By comparing this with the convolution of the grid and the same PDF that is used by `MCFM`, we can check if any errors occur during the grid calculation, especially from the subprocess decomposition or grid parameters. Figure 2 shows ratio plots between grid and standard calculation. Evidently, the error is strictly smaller than 0.006% for the leading jet grid and smaller than 0.017% for the subleading jet grid. This very small discrepancy is likely an artifact of the interpolation and validates the used subprocess decomposition.

4 Results

4.1 Comparison to ATLAS data

To compare our results to experimental measurements, we use ATLAS measurements of Z+jet production in bins of leading and sub-leading jet rapidities [6]. Their analysis comprises the $\sqrt{s} = 7$ TeV 2011 dataset corresponding to an integrated luminosity of 4.6 fb^{-1}. The values used for the following plots were obtained from the Durham HepData repository[1]. The ATLAS detector is described in detail in [13].

Figure 3 compares the absolute differential cross sections for binning in both leading and subleading jet rapidity.

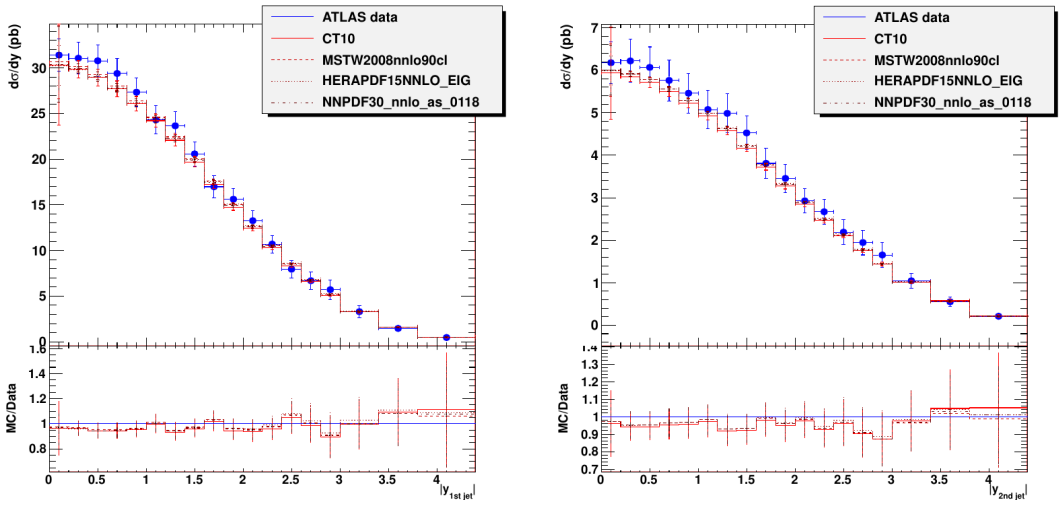

(a) Leading jet (b) Subleading jet

FIG. 3. Comparison between ATLAS measurements [6] and calculated values for the Z+jet cross section in bins of the (a) leading or (b) subleading jet rapidity $|y|$. Used PDF sets are from CT10 [2], HERAPDF [14], NNPDF [1] and MSTW2008 [3]. MC error bars are from PDF uncertainty only.

While the predictions are, within experimental error, in overall agreement with the measurements, there is a clear tendency of lower cross sections at small jet rapidities. This tendency is also present in some theory predictions listed in the atlas paper, namely MC@NLO and SHERPA but not in ALPGEN.

The cross section does not vary greatly between calculations using different PDF sets.

[1] `http://hepdata.cedar.ac.uk/view/ins1230812`

Except for lower absolute cross sections due to the requirement of at least one subleading jet in the final state, there is no qualitative difference between leading and subleading measurements and predictions.

4.2 Subprocess Contributions

The first step to assess the sensitivity of the generated cross section to the gluon PDF is to consider the relative contributions of subprocesses involving gluons. These are listed in Table V for both generated grids, where the subprocesses have been grouped into quark-quark (QQ), quark-gluon (QG) and gluon-gluon (GG) processes. For these calculations, the CT10 PDF set was used.

	Leading jet	Subleading jet
QQ	24.70%	26.69%
QG	78.51%	67.88%
GG	-3.20%	5.42%

TABLE V. Relative contributions to total cross section from different subprocesses using leading and subleading jet rapidity grids.

Clearly, the largest contribution comes from quark-gluon processes with only minor differences between leading and subleading jet calculations. This shows at least the potential for sensitivity to the gluon PDF.

To investigate the dependency on jet rapidity, Figure 4 shows the relative contributions from each subprocess group as a function of the rapidity bins.

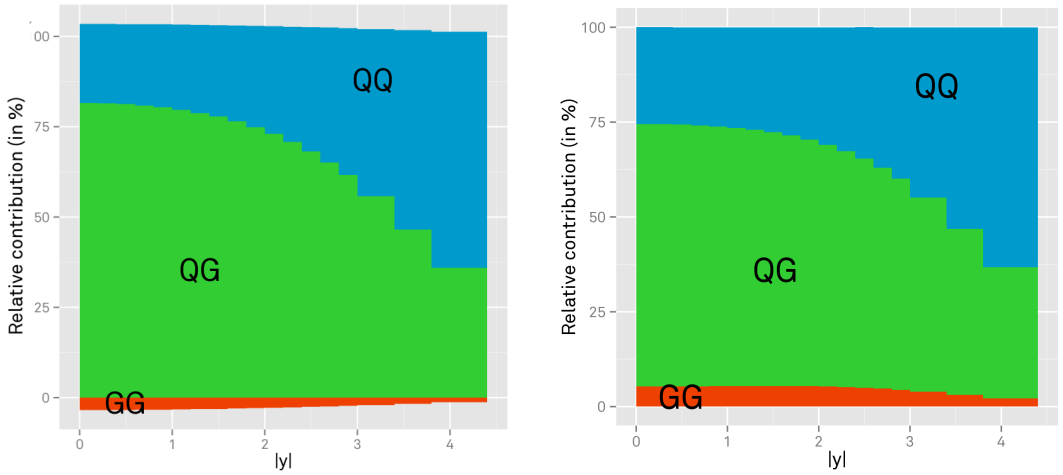

(a) Leading jet

(b) Subleading jet

FIG. 4. Relative contributions to the cross section from different subprocesses with binning in the (a) leading and (b) subleading jet rapidity.

Again, the results look very similar between leading and subleading calculations. Primarily, the relative contribution from quark-gluon processes decreases for high jet rapidities in favour of quark-quark processes. This shows the possibility of a sensitivity to the gluon PDF in the shape of the measured differential cross section.

4.3 Correlation between cross section and gluon PDF

The following correlations were calculated by convoluting the grid with each of the eigenvectors typically distributed with the PDF. Both the resulting cross sections and the corresponding gluon density at a number of points in x were saved and passed to the `LHAPDF 6` function `correlation()`.

The resulting correlations with the total and binned cross section are plotted in Figures 5, 6 and 7.

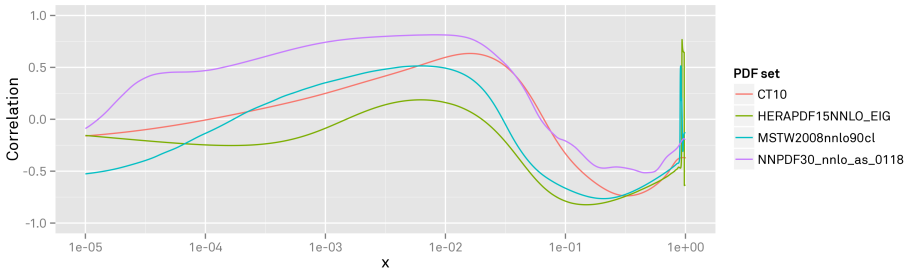

(a) Leading jet

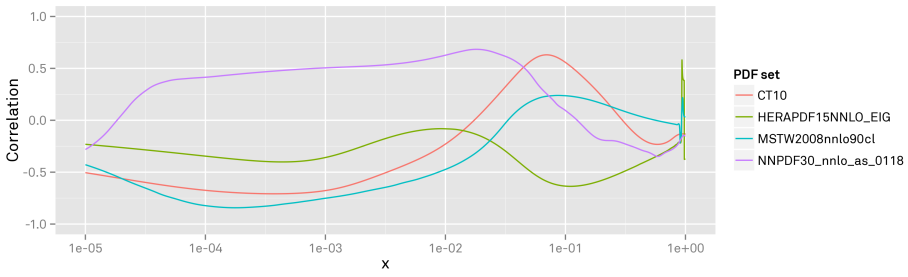

(b) Subleading jet

FIG. 5. Correlation between gluon PDF and calculated total cross section as a function of the gluons fractional momentum x for different PDF sets. The gluon PDF is evaluated at $Q = 100$ GeV

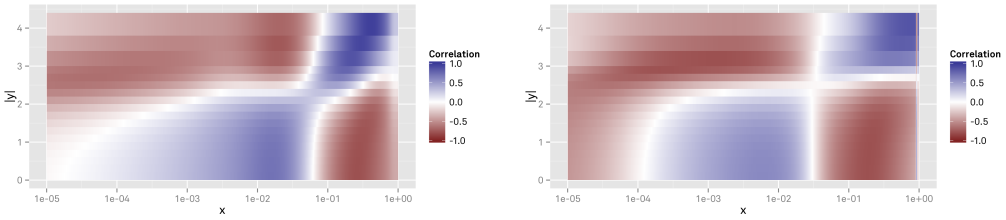

(a) CT10

(b) MSTW2008nnlo90cl

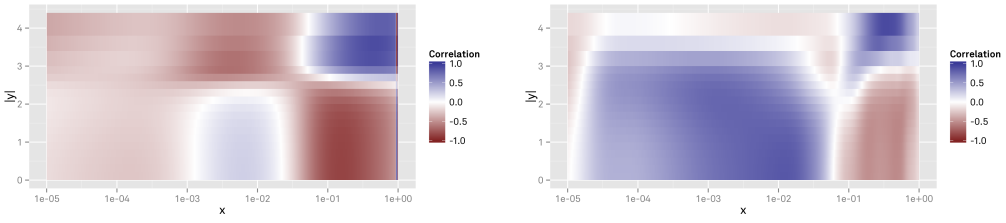

(c) HERAPDF15NNLO_EIG

(d) NNPDF30_nnlo_as_0118

FIG. 6. Correlation between gluon PDF and calculated cross section. The horizontal axis corresponds to the gluons fractional momentum x, the vertical axis to rapidity bins $|y|$ of the leading jet. Dark blue and red stand for a strong correlation and anticorrelation, respectively.

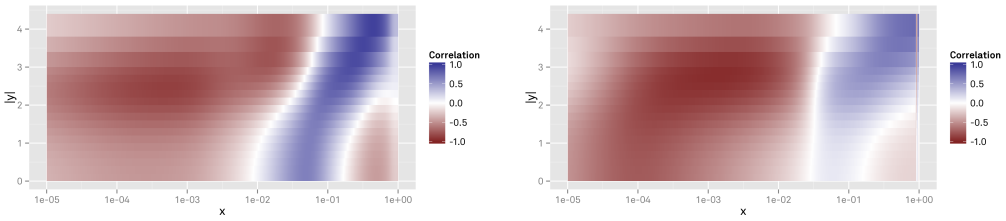

(a) CT10

(b) MSTW2008nnlo90cl

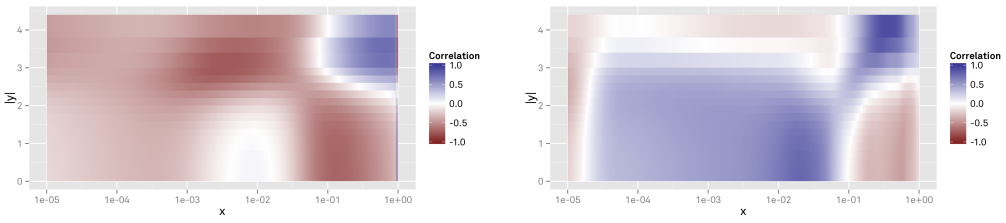

(c) HERAPDF15NNLO_EIG

(d) NNPDF30_nnlo_as_0118

FIG. 7. Correlation between gluon PDF and calculated cross section. The horizontal axis corresponds to the gluons fractional momentum x, the vertical axis to rapidity bins $|y|$ of the subleading jet. Dark blue and red stand for a strong correlation and anticorrelation, respectively.

While the exact shape of the correlation varies with the chosen PDF set, especially so for bin-by-bin correlations, there seems to be a common higher correlation with the gluon PDF at fractional momenta at around 0.2 and 0.01. The fluctuations for very high x are likely due to the very small and sometimes even negative values of the

gluon PDF in this region. Moreover, for some PDF sets deviations in the gluon PDF in a sensitive kinematic regions could account for the observed tendency for a wider rapidity distribution.

5 Conclusion

This report presents the generation of an interpolation grid for Z+jet production in bins of jet rapidity at the ATLAS detector and investigates the sensitivity of experimental data to the gluon PDF using this grid. We find that gluon-quark and gluon-gluon processes give the largest contribution to the production cross section. Both the total cross section and rapidity distribution are strongly correlated with the value of the gluon PDF in different kinematical regions, which shows a potential for using this process in PDF fits in order to constrain the gluon PDF.

Once the reason for the high deviations between standard and grid calculations for a dynamic factorisation scale determined, the results of this analysis should be checked with this more realistic grid.

A possible extension of this work would be to use the generated grids for inclusion of the ATLAS measurements into PDF fits. This could be done using the HERAfitter package, which already uses APPLgrid to fit inclusive jet and Drell-Yan data. The transverse momentum spectrum could be investigated in a similar way.

Acknowledgements

I'd like to thank my supervisor Pavel Starovoitov and the rest of the DESY ATLAS group for a lot of support and a very friendly atmosphere. Moreover, I'm very grateful to the organizing team of the summer student programme 2014 for making this experience possible.

Appendix A: input.DAT

```
'6.8'                   [file version number]

[Flags to specify the mode in which MCFM is run]
-1                      [nevtrequested]
.false.                 [creatent]
.false.                 [skipnt]
.false.                 [dswhisto]
.true.                  [creategrid]
.false.                 [writetop]
.false.                 [writedat]
.false.                 [writegnu]
.true.                  [writeroot]
.false.                 [writepwg]

[General options to specify the process and execution]
41                      [nproc]
'tota'                  [part]
'run'                   [runstring]
7000d0                  [sqrts in GeV]
+1                      [ih1 =1 for proton and -1 for antiproton]
+1                      [ih2 =1 for proton and -1 for antiproton]
125.36d0                [hmass]
91d0                   [scale:QCD scale choice]
91d0                   [facscale:QCD fac_scale choice]
'none'                    [dynamicscale]
.false.                 [zerowidth]
.false.                 [removebr]
4                       [itmx1, number of iterations for pre-conditioning]
200000                  [ncall1]
10                      [itmx2, number of iterations for final run]
200000                  [ncall2]
28                      [ij]
.false.                 [dryrun]
.true.                  [Qflag]
.true.                  [Gflag]

[Heavy quark masses]
173.34d0                [top mass]
4.65d0                  [bottom mass]
1.275d0                 [charm mass]

[Pdf selection]
'cteq66m'               [pdlabel]
4                       [NGROUP, see PDFLIB]
46                      [NSET - see PDFLIB]
CT10.LHgrid             [LHAPDF group]
0                       [LHAPDF set]

[Jet definition and event cuts]
66d0                    [m34min]
116d0                   [m34max]
10d0                    [m56min]
7000d0                  [m56max]
.true.                  [inclusive]
'ankt'                  [algorithm]
30d0                    [ptjet_min]
0d0                     [|etajet|_min]
4.4d0                   [|etajet|_max]
0.4d0                   [Rcut_jet]
.true.                  [makecuts]
20d0                    [ptlepton_min]
2.47d0                  [|etalepton|_max]
1.37d0,1.52d0           [|etalepton|_veto]
```

```
0d0                     [ptmin_missing]
20d0                    [ptlepton(2nd+)_min]
2.47d0                  [|etalepton(2nd+)|_max]
1.37d0,1.52d0           [|etalepton(2nd+)|_veto]
0d0                     [minimum (3,4) transverse mass]
0.5d0                   [R(jet,lept)_min]
0.2d0                   [R(lept,lept)_min]
0d0                     [Delta_eta(jet,jet)_min]
.false.                 [jets_opphem]
0                       [lepbtwnjets_scheme]
0d0                     [ptmin_bjet]
99d0                    [etamax_bjet]

[Settings for photon processes]
.false.                 [fragmentation included]
'GdRG__LO'              [fragmentation set]
80d0                    [fragmentation scale]
20d0                    [ptmin_photon]
2.5d0                   [etamax_photon]
20d0                    [ptmin_photon(2nd)]
20d0                    [ptmin_photon(3rd)]
0d0                     [R(photon,lept)_min]
0.4d0                   [R(photon,photon)_min]
0.4d0                   [R(photon,jet)_min]
0.4d0                   [cone size for isolation]
0.5d0                   [epsilon_h, energy fraction for isolation]

[Anomalous couplings of the W and Z]
0.0d0                   [Delta_g1(Z)]
0.0d0                   [Delta_K(Z)]
0.0d0                   [Delta_K(gamma)]
0.0d0                   [Lambda(Z)]
0.0d0                   [Lambda(gamma)]
0.0d0                   [h1(Z)]
0.0d0                   [h1(gamma)]
0.0d0                   [h2(Z)]
0.0d0                   [h2(gamma)]
0.0d0                   [h3(Z)]
0.0d0                   [h3(gamma)]
0.0d0                   [h4(Z)]
0.0d0                   [h4(gamma)]
2.0d0                   [Form-factor scale, in TeV]

[Anomalous width of the Higgs]
1d0                     [Gamma_H/Gamma_H(SM)]

[How to resume/save a run]
.false.                 [readin]
.false.                 [writeout]
''                      [ingridfile]
''                      [outgridfile]

[Technical parameters that should not normally be changed]
.false.                 [debug]
.true.                  [verbose]
.false.                 [new_pspace]
.false.                 [virtonly]
.false.                 [realonly]
.true.                  [spira]
.false.                 [noglue]
.false.                 [ggonly]
.false.                 [gqonly]
.false.                 [omitgg]
.false.                 [vanillafiles]
1                       [nmin]
2                       [nmax]
.true.                  [clustering]
.false.                 [realwt]
0                       [colourchoice]
1d-2                    [rtsmin]
1d-4                    [cutoff]
0.1d0                   [aii]
0.1d0                   [aif]
0.1d0                   [afi]
1d0                     [aff]
1d0                     [bfi]
1d0                     [bff]
```

References

[1] Richard D. Ball et al. "Parton distributions with QED corrections". In: *Nucl.Phys.* B877 (2013), pp. 290–320. DOI: 10.1016/j.nuclphysb.2013.10.010. arXiv: 1308.0598 [hep-ph].

[2] Jun Gao et al. "The CT10 NNLO Global Analysis of QCD". In: *Phys. Rev. D* 89 (Aug. 2014), p. 033009. DOI: 10.1103/PhysRevD.89.033009. arXiv: 1302.6246v2 [hep-ph].

[3] A. D. Martin et al. "Parton distributions for the LHC". In: (2009). cite arxiv:0901.0002 Comment: 157 pages, 70 figures. Code can be found at http://projects.hepforge.org/mstwpdf/ and in LHAPDF V5.7.0. v3: final version published in EPJC with extended Section 12.

[4] Tancredi Carli et al. *A posteriori inclusion of parton density functions in NLO QCD final-state calculations at hadron colliders: The APPLGRID Project*. Nov. 2009. arXiv: 0911.2985v1 [hep-ph].

[5] J. Campbell et al. "Associated Production of a Z Boson and a Single Heavy-Quark Jet". In: *Phys.Rev.D* 69 (Jan. 2004), p. 074021. DOI: 10.1103/PhysRevD.69.074021. arXiv: hep-ph/0312024v2 [hep-ph].

[6] M Pinamonti, ATLAS Collaboration, et al. "Measurement of the production cross section of jets in association with a Z boson in pp collisions at sqrt (s)= 7 TeV with the ATLAS detector". In: (2013).

[7] Guido Altarelli. "Partons in Quantum Chromodynamics". In: *Phys.Rept.* 81 (1982), p. 1. DOI: 10.1016/0370-1573(82)90127-2.

[8] John C. Collins, Davison E. Soper, and George Sterman. "Factorization of Hard Processes in QCD". In: (2004). cite arxiv:hep-ph/0409313 Comment: 100 pages, 27 figures. Authors' affiliations updated compared with published version.

[9] J Butterworth et al. "Les Houches 2013: Physics at TeV Colliders: Standard Model Working Group Report". In: *arXiv preprint arXiv:1405.1067* (2014).

[10] G. P. Salam and J. Rojo. "A Higher Order Perturbative Parton Evolution Toolkit (HOPPET)." In: *Computer Physics Communications* 180.1 (Sept. 25, 2009), pp. 120–156.

[11] Matteo Cacciari, Gavin P. Salam, and Gregory Soyez. "FastJet user manual". In: *Eur.Phys.J.* C72 (2012), p. 1896. DOI: 10.1140/epjc/s10052-012-1896-2. arXiv: 1111.6097 [hep-ph].

[12] Matteo Cacciari, Gavin P. Salam, and Gregory Soyez. *The anti-k_t jet clustering algorithm*. arxiv:0802.1189. 2008. DOI: 10.1088/1126-6708/2008/04/063.

[13] G. Aad et al. "The ATLAS Experiment at the CERN Large Hadron Collider". In: *JINST* 3 (2008), S08003. DOI: 10.1088/1748-0221/3/08/S08003.

[14] The H1 and ZEUS Collaborations. *Combined Measurement and QCD Analysis of the Inclusive ep Scattering Cross Sections at HERA*. arxiv:0911.0884. 2009. DOI: 10.1007/JHEP01(2010)109.